Monthly Notices
of the
ROYAL ASTRONOMICAL SOCIETY

Mon. Not. R. Astron. Soc. **407,** 1188–1202 (2010) doi:10.1111/j.1365-2966.2010.17004.x

Searching for dark matter in X-rays: how to check the dark matter origin of a spectral feature

Alexey Boyarsky,[1,2] Oleg Ruchayskiy,[1] Dmytro Iakubovskyi,[2★] Matthew G. Walker,[3] Signe Riemer-Sørensen[4] and Steen H. Hansen[4]

[1]*Ecole Polytechnique Fédérale de Lausanne, FSB/ITP/LPPC, BSP CH-1015, Lausanne, Switzerland*
[2]*Bogolyubov Institute for Theoretical Physics, Metrologichna str., 14-b, Kiev 03680, Ukraine*
[3]*Institute of Astronomy, University of Cambridge, Cambridge CB3 0HA*
[4]*Dark Cosmology Centre, Niels Bohr Institute, University of Copenhagen, Juliane Maries Vej 30, DK-2100 Copenhagen, Denmark.*[†]

Accepted 2010 May 5. Received 2010 April 23; in original form 2010 January 21

ABSTRACT

A signal from decaying dark matter (DM) can be unambiguously distinguished from spectral features of astrophysical or instrumental origin by studying its spatial distribution. We demonstrate this approach by examining the recent claim of Loewenstein and Kusenko regarding the possible DM origin of the 2.5 keV line in *Chandra* observations of the Milky Way satellite known as Willman 1. Our conservative strategy is to adopt, among reasonable mass estimates derived here and in the literature, a relatively large dark mass for Willman 1 and relatively small dark masses for the comparison objects. In light of the large uncertainty in the actual DM content of Willman 1, this strategy provides minimum exclusion limits on the DM origin of the reported signal. We analyse archival observations by *XMM–Newton* of M31 and Fornax dwarf spheroidal galaxy (dSph) and *Chandra* observations of Sculptor dSph. By performing a conservative analysis of X-ray spectra, we show the absence of a DM decay line with parameters consistent with those of Loewenstein and Kusenko. For M31, the observations of the regions between 10 and 20 kpc from the centre, where the uncertainties in the DM distribution are minimal, make a strong exclusion at the level above 10σ. The Fornax dSph provides a $\sim 3.3\sigma$ exclusion instead of a predicted 4σ detection, and the Sculptor dSph provides a 3σ exclusion instead of a predicted 2.5σ detection. The observations of the central region of M31 (1–3 kpc off-centre) are inconsistent with having a DM decay line at more than 20σ if one takes the most conservative among the best physically motivated models. The minimal estimate for the amount of DM in the central 40 kpc of M31 is provided by the model of Corbelli et al., assuming the stellar disc's mass to light ratio ~ 8 and almost constant DM density within a core of 28 kpc. Even in this case one gets an exclusion at 5.7σ from central region of M31, whereas modelling *all* processed data from M31 and Fornax produces more than 14σ exclusion. Therefore, despite possible systematic uncertainties, we exclude the possibility that the spectral feature at ~ 2.5 keV found in Loewenstein and Kusenko is a DM decay line. We conclude, however, that the search for DM decay line, although demanding prolonged (up to 1 Ms) observations of well-studied dSphs, M31 outskirts and other similar objects, is rather promising, as the nature of a possible signal can be checked. An (expected) non-observation of a DM decay signal in the planned observations of Willman 1 should not discourage further dedicated observations.

Key words: galaxies: individual: M31 – galaxies: individual: Fornax – galaxies: individual: Sculptor – galaxies: individual: Willman 1 – dark matter – X-rays: diffuse background.

★E-mail: yakubovskiy@bitp.kiev.ua

†The Dark Cosmology Centre is funded by the Danish National Research Foundation.

1 INTRODUCTION

Modern astrophysical and cosmological data strongly indicate that a significant amount of matter in the Universe exists in the form of DM. The nature of DM remains completely unknown and its existence presents one of the major challenges to modern physics. It is commonly believed that the DM is made of particles.[1] However, the Standard Model of elementary particles fails to provide a DM candidate. Therefore the hypothesis of a particle nature of DM implies extension of the Standard Model.

Weakly interacting massive particles (WIMPs) are probably the most popular class of DM candidates. They appear in many extensions of the Standard Model (see e.g. Bertone, Hooper & Silk 2005; Hooper 2009). These stable particles interact with the SM sector with roughly electroweak strength (Lee & Weinberg 1977). To provide a correct DM abundance, WIMPs should have mass in the GeV range. A significant experimental effort is devoted to the detection of the interaction of WIMPs in the Galaxy's DM halo with laboratory nucleons (*direct detection experiments*; see e.g. Baudis 2007) or to finding their annihilation signal in space (*indirect detection experiments*; see e.g. Carr, Lamanna & Lavalle 2006; Bergstrom 2008; Hooper & Baltz 2008).

Another large class of DM candidates are *superweakly* interacting particles (so-called *super-WIMPs*), i.e. particles, whose interaction strength with the SM particles is much more feeble than the weak one. Super-WIMPs appear in many extensions of the Standard Model: extensions of the SM by right-handed neutrinos (Dodelson & Widrow 1994; Asaka, Blanchet & Shaposhnikov 2005; Lattanzi & Valle 2007), supersymmetric theories (Takayama & Yamaguchi 2000; Feng, Rajaraman & Takayama 2003; Feng, Su & Takayama 2004; Buchmuller et al. 2007), models with extra dimensions (Feng et al. 2003) and string-motivated models (Conlon & Quevedo 2007). The feeble interaction strength makes the laboratory detection of super-WIMPs challenging (see e.g. Bezrukov & Shaposhnikov 2007). On the other hand, many super-WIMP particles possess a *two-body radiative decay* channel: DM $\rightarrow \gamma + \nu$, $\gamma + \gamma$, producing a photon with energy $E_\gamma = M_{\rm DM}/2$. One can therefore search for the presence of such a monochromatic line with energy in the spectra of DM-containing objects (Abazajian, Fuller & Tucker 2001; Dolgov & Hansen 2002). Although the lifetime of any realistic decaying DM is much longer than the lifetime of the Universe (see e.g. Boyarsky & Ruchayskiy 2008), the huge amount of potentially decaying DM particles in a typical halo means a potentially detectable decay signal in the spectra of DM-dominated objects. Searching for such a line provides a major way of *detection of super-WIMP DM particles*.

The strategy of the search for decaying DM signal drastically differs from its annihilation counterpart. Indeed, the *decay* signal is proportional to the *DM column density* – integral of a DM distribution $\rho_{\rm DM}$ along the line of sight $\mathcal{S} = \int_{\rm l.o.s.} \rho_{\rm DM}(r){\rm d}r$ as opposed to $\int_{\rm l.o.s.} \rho^2_{\rm DM}(r){\rm d}r$ in the case for annihilating DM. The DM column density varies slowly with the mass of DM objects (Boyarsky et al. 2006b, 2009a) and as a result a vast variety of astrophysical objects of different nature would produce a comparable decay signal (Boyarsky et al. 2006b, 2009a; Bertone et al. 2007). Therefore, (i) without sacrificing the expected signal one has a freedom of choosing observational targets, avoiding complicated astrophysical backgrounds; (ii) if a candidate line is found, its surface brightness profile may be measured (as it does not decay quickly away from the centres of the objects) and distinguished from astrophysical lines that usually decay in outskirts of galaxies and clusters. Moreover, any tentative detection in one object would imply a signal of certain (comparable) signal-to-noise ratio (S/N) from a number of other objects. This can be checked and the signal can either be unambiguously confirmed to be that of DM decay origin or ruled out. This allows to distinguish the decaying DM line from any possible astrophysical background and therefore makes astrophysical search for the decaying DM *another type of a direct detection experiment*.

In this paper, we demonstrate the power of this approach. We check the recent conjecture by Loewenstein & Kusenko (2010, hereafter LK10), who reported that a spectral feature at 2.51 ± 0.07 keV with the flux $(3.53 \pm 1.95) \times 10^{-6}$ photons cm^{-2} s^{-1} (all errors at 68 per cent confidence level) in the spectrum of the Milky Way satellite known as Willman 1 (Willman et al. 2005) may be interpreted as a DM decay line. According to LK10, the line with such parameters is marginally consistent the restrictions on decaying DM from some objects (see e.g. Loewenstein, Kusenko & Biermann 2009; Riemer-Sorensen & Hansen 2009 or the restrictions from the 7 ks observation of Ursa Minor dwarf spheroidal in Boyarsky, Nevalainen & Ruchayskiy 2007b). The results of other works (e.g. Watson et al. 2006; Abazajian et al. 2007; Boyarsky et al. 2008a, hereafter B08) are inconsistent at 3σ level with having 100 per cent of decaying DM with the best-fitting parameters of LK10. However, it is hard to exclude completely new unknown systematic uncertainties in the DM mass estimates and therefore in expected signal, from any given object. To this end, in this work we explicitly check for a presence of a line with parameters, specified above, by using archival observations by *XMM–Newton* and *Chandra* of several objects, where comparable or stronger signal was expected. We compare the signals from several objects and show that the spatial (angular) behaviour of the spectral feature is inconsistent with its DM origin so strongly, that systematic uncertainties cannot affect this conclusion. We also discuss a possible origin of the spectral feature of LK10.

2 CHOICE OF OBSERVATIONAL TARGETS

The particle flux of the decaying DM (in photons cm^{-2} × s) is given by

$$F_{\rm DM} = \frac{\Gamma}{4\pi m_{\rm DM}} \frac{M^{\rm fov}_{\rm DM}}{D^2_{\rm L}} = \frac{\Gamma}{4\pi m_{\rm DM}} \Omega_{\rm fov} \mathcal{S}, \quad (1)$$

where $m_{\rm DM}$ is the mass of the DM particle, Γ is the decay rate to photons (depending on the particular model of decaying DM), $M^{\rm fov}_{\rm DM}$ is the DM mass within the instrument's field-of-view (FOV) $\Omega_{\rm fov}$ and $D_{\rm L}$ is the luminous distance towards the object.[2]

2.1 Willman 1 signal

In LK10 the signal was extracted from the central 5 arcmin of the Willman 1 observation. Assuming the DM origin of this signal, the observed flux $(3.53 \pm 1.95) \times 10^{-6}$ photons cm^{-2} s^{-1} corresponds to $F_{\rm W1} = (4.50 \pm 2.5) \times 10^{-8}$ photons cm^{-2} s^{-1} arcmin^{-2} flux per unit solid angle. The mass within the FOV of the observation of Willman 1 was estimated in LK10 to be $M^{\rm fov}_{\rm W1} = 2 \times 10^6\,{\rm M}_\odot$, using the best-fitting values from Strigari et al. (2008). Taking the luminous distance to the object to be $D_{\rm L} = 38$ kpc, the average

[1] Although more exotic possibilities [such as e.g. primordial black holes; Carr (2005)] exist.

[2] Equation (1) is valid for all objects whose size is much smaller than $D_{\rm L}$.

DM column density of Willman 1 is $\mathcal{S}_{\rm W1} \simeq 208.5\,{\rm M}_\odot\,{\rm pc}^{-2}$ (see however discussion in the Section 5). To check the presence of a DM decay line, we should look for targets with comparable signal.

The S/N for a weak line observed against a featureless continuum is given by (see e.g. discussion in Boyarsky et al. 2007a)

$$({\rm S/N}) \propto \mathcal{S}\sqrt{t_{\rm exp} A_{\rm eff} \Omega_{\rm fov} \Delta E}, \quad (2)$$

where $\mathcal{S}$ is the average DM column density within an instrument's FOV $\Omega_{\rm fov}, t_{\rm exp}$ is the exposure time, $A_{\rm eff}$ is an effective area of the detector and ΔE is the spectral resolution (notice that the line in question has a much smaller intrinsic width than the spectral resolution of *Chandra* and *XMM–Newton*). For the purpose of our estimate we consider the effective areas of *XMM–Newton* MOS cameras and *Chandra* ACIS-I (as well as their spectral resolution) to be approximately equal, and effective area of PN camera is two times bigger.[3]

2.2 Galactic contribution

The contribution of the Milky Way's DM halo along the line of sight should also be taken into account, when estimating the DM decay signal.[4] Using a pseudo-isothermal profile

$$\rho_{\rm iso}(r) = \frac{\rho_{\rm c}}{1 + r^2/r_{\rm c}^2}, \quad (3)$$

with parameters, adopted in Boyarsky et al. (2006b, 2007b) ($r_{\rm c} = 4\,{\rm kpc}$, $\rho_{\rm c} = 33.5 \times 10^6\,{\rm M}_\odot\,{\rm kpc}^3, {\rm r}_\odot = 8\,{\rm kpc}$), the corresponding Milky Way column density in the direction of Willman 1 (120.°7 off Galactic centre) is $73.9\,{\rm M}_\odot\,{\rm pc}^{-2}$. As demonstrated in Boyarsky et al. (2008b), the value of DM column density computed with this DM density profile coincides with the best-fitting Navarro–Frenk–White (NFW; Navarro, Frenk & White 1997) profiles of Klypin, Zhao & Somerville (2002) and Battaglia et al. (2005) within few per cent for the off-centre angle $\phi \gtrsim 90^\circ$. Other DM distributions produce systematically larger values of DM column density. For example, the best-fitting pseudo-isothermal profile of Kerins et al. (2001) would corresponds to an additional Milky Way contribution $\sim 119\,{\rm M}_\odot\,{\rm pc}^{-2}$ in the direction of Willman 1. The comparison between the DM column densities of several objects with that of Milky Way in their directions is shown in Fig. 1.

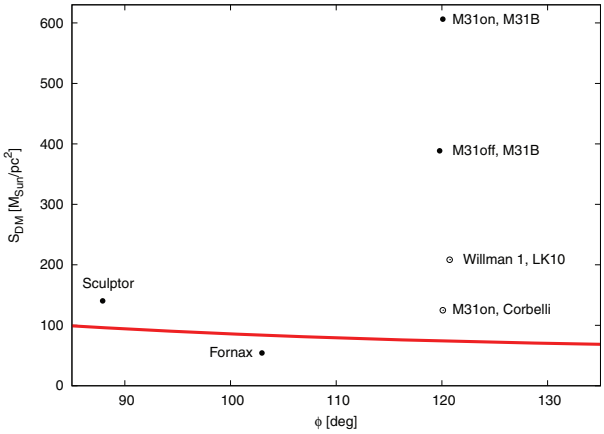

Figure 1. Comparison of DM column densities of the Milky Way (red solid line) with the density profiles of M31, Fornax and Sculptor dSphs, discussed in the text. The DM column density estimate for Willman 1 is based on the 'optimistic' DM density profile from Strigari et al. (2008), used in LK10 (see Section 5.1 for discussion). The angle ϕ marks the direction off Galactic centre [for an object with galactic coordinates (l, b) $\cos\phi = \cos l \cos b$].

3 *XMM–Newton* DATA ANALYSIS

For each *XMM–Newton* observation, we extracted both EPIC MOS and PN spectra.[5] We select events with PATTERN $<=12$ for MOS and PATTERN $==0$ for PN camera and use FLAG $==0$. We used SAS task edetect_chain to exclude point sources, detected with the likelihood values above 10 (about 4σ). For EPIC PN camera, bright strips with out-of-time (OOT) events were also filtered out, following the standard procedure.[6] We imposed stringent flare screening criteria. To identify 'good time intervals' we performed a light-curve cleaning, by analysing temporal variability in the hard ($E > 10\,{\rm keV}$) X-ray band (as described e.g. in Read & Ponman 2003; Nevalainen, Markevitch & Lumb 2005; Carter & Read 2007). The resulting light curves were inspected 'by eye' and additional screening of soft proton flares was performed by employing a method similar to that described in e.g. Leccardi & Molendi (2008) and Kuntz & Snowden (2008) (i.e. by rejecting periods when the count rate deviated from a constant by more than 2σ). The extracted spectra were checked for the presence of residual soft proton contaminants by comparing count rates in and out of FOV (De Luca & Molendi 2004; Leccardi & Molendi 2008).[7] In all spectra that we extracted the ratio of count rates in and out of FOV did not exceed 1.13 which indicates thorough soft proton flare cleaning (cf. Leccardi & Molendi 2008).

Following the procedure, described in Carter & Read (2007) we extracted the filter-wheel closed background[8] from the same region as signal (in detector coordinates). The background was further renormalized based on the $E > 10$ keV band count rates of the extracted spectra. The resulting source and background spectra are grouped by at least 50 counts per bin using FTOOL (Irby 2008) command grppha.

The extracted spectra with subtracted instrumental background were fitted by the power-law model of XSPEC in the energy range 2.1–8.0 keV data for MOS and 2.1–7.2 keV for the PN camera. This choice of the *baseline model* is justified by the fact that for all considered objects we expect no intrinsic X-ray emission above 2 keV and therefore the observed signal is dominated by the extragalactic diffuse X-ray background (XRB) with the power-law slope $\Gamma = 1.41 \pm 0.06$ and the normalization $(9.8 \pm 1.0) \times 10^{-7}$ photons cm^{-2} s^{-1} keV^{-1} arcmin^{-2} at 1 keV (90 per cent CL errors) (see e.g. Lumb et al. 2002; De Luca & Molendi 2004; Nevalainen et al. 2005; Hickox & Markevitch 2006; Carter & Read 2007; Moretti et al. 2009). Galactic contribution (both in absorption and in emission) is negligible at these energies and we do not take it into account in what follows. For all considered observations

[3] See e.g. http://xmm.esa.int/external/xmm_user_support/documentation/uhb/node32.html and http://cxc.harvard.edu/ccr/proceedings/07_proc/presentations/drake/.

[4] Note that both in LK10 and in this work only instrumental (particle) background has been subtracted from the observed diffuse spectra.

[5] We use SAS version 9.0.0 and XSPEC 12.6.0.

[6] As described for example at http://xmm.esac.esa.int/sas/current/documentation/threads/EPIC_OoT.shtml.

[7] We use the script http://xmm2.esac.esa.int/external/xmm_sw_cal/background/Fin_over_Fout De Luca & Molendi (2004) provided by the *XMM–Newton* EPIC Background working group.

[8] Available at http://xmm2.esac.esa.int/external/xmm_sw_cal/background/filter_closed/index.shtml.

Table 1. Best-fitting values of power-law index and normalization for each *XMM–Newton* observation analysed in this paper. The systematic uncertainty is included (see text). In M31on region, power-law index for different observations is chosen to be the same, because they point to the same spatial region.

ObsID	PL index	PL norm, 10^{-4} ph. cm^{-2} s^{-1} keV^{-1}) at 1 keV (MOS1/MOS2/PN)	χ^2/d.o.f.
		M31on observations	
0109270101	1.33	5.71/5.80/7.88	1328/1363
0112570101	–	5.37/6.12/6.86	–
0112570401	–	6.13/6.66/6.37	–
		M31off observation	
0402560301	1.46	6.28/6.12/9.97	895/997
		M31out observations	
0511380101	1.53	2.75/2.88/3.89	875/857
0109270401	1.47	5.02/4.41/5.22	606/605
0505760401	1.27	1.91/2.04/2.47	548/528
0505760501	1.28	2.25/1.85/3.03	533/506
0402561301	1.57	2.94/3.10/3.95	489/515
0402561401	1.47	4.33/3.58/4.47	751/730
0402560801	1.55	5.22/4.49/5.83	902/868
0402561501	1.44	2.70/4.29/6.67	814/839
0109270301	1.39	4.29/4.58/3.75	413/436
		Fornax observation	
0302500101	1.52	4.46/4.02/3.78	938/981

power-law model provided a very good fit, fully consistent with the above measurements of XRB. The power-law index was fixed to be the same for all cameras (MOS1, MOS2 and PN), observing the same spatial region, while the normalization was allowed to vary independently to account for the possible off-axis calibration uncertainties between the different cameras (see e.g. Mateos et al. 2009; Carter, Sembay & Read 2010). The best-fitting values of the power-law index and normalizations are presented in Table 1.

To check for the presence of the LK10 line in the spectra, we added a narrow ($\Delta E/E \sim 10^{-3}$) Gaussian line (XSPEC model Gaussian) to the baseline power-law model. Assuming the DM origin of this line, we fix its normalization at the level $F_{\rm W1}$, derived in LK10, multiplied by the ratio of total (including Milky Way contribution) DM column densities and instrument's FOV. We vary the position of the line in the interval corresponding to the 3σ interval of LK10: 2.30–2.72 keV. Equation (2) allows to estimate the expected significance of the line.

When searching for weak lines, one should also take into account uncertainties arising from the inaccuracies in the calibration of the detector response and gain. This can lead to systematic residuals caused by calibration inaccuracies, at the level $\sim$5 per cent of the model flux (some of them having edge-like or even line-like shapes) (see e.g. Kirsch et al. 2002, 2004) as well as discussion in Boyarsky, Ruchayskiy & Markevitch (2008c) for similar uncertainties in *Chandra*. To account for these uncertainties we perform the above procedure with the 5 per cent of the model flux added as a systematic error (using XSPEC command systematic).

4 ANDROMEDA GALAXY

4.1 Dark matter content of M31

The Andromeda galaxy is the closest spiral galaxy to the Milky Way. Its DM content has been extensively studied over the years (see e.g. Kerins et al. 2001; Klypin et al. 2002; Widrow & Dubinski 2005; Geehan et al. 2006; Tempel, Tamm & Tenjes 2007; Chemin, Carignan & Foster 2009; Corbelli et al. 2010, and references therein) for an incomplete list of recent works. The total dynamical mass (out to $\sim$40 kpc) can be determined from the rotation curve measured from H I kinematics. The major uncertainty in determination of DM content is then related to a separation of contributions of baryonic (stellar bulge and especially,extended stellar disc) and dark components to the total mass.[9] The baryonic mass is often obtained from the (deprojected) surface brightness profile (optical or infrared), assuming certain mass-to-light ratio for the luminous matter in the bulge and the disc of a galaxy.

B08 analysed DM distributions of M31, existing in the literature at that time in order to provide the most conservative estimate of the expected DM decay signal. The DM column density $\mathcal{S}$ in more than 10 models from the works (Kerins et al. 2001; Klypin et al. 2002; Widrow & Dubinski 2005; Geehan et al. 2006; Tempel et al. 2007) turns out to be consistent within a factor of $\sim$2 for off-centre distances greater than $\sim$1 kpc (see grey lines in Fig. 2). The most conservative estimate of DM column density was provided by one of the models of Widrow & Dubinski (2005) (called in that work M31B), marked as red solid line on Fig. 2.

Recently two new H I surveys of the disc of M31 were performed (Chemin et al. 2009; Corbelli et al. 2010) and new data on mass distribution of M31 became available.[10] In Chemin et al. (2009) modelling of H I rotation curve between $\sim$0.3 and 38 kpc was performed. Chemin et al. (2009) used *R*-band photometric information (Walterbos & Kennicutt 1987, 1988) to determine the relative contribution of the stellar disc and the bulge. Based on this information and taking into account foreground and internal extinction/reddening effects (see section 8.2.2 in Chemin et al. 2009, for details) they determined mass-to-light ratio, using stellar population

[9] Some works also take into account a presence of supermassive black hole in the centre of a galaxy (see e.g Widrow & Dubinski 2005) and additional contribution of a gaseous disc (cf. Chemin et al. 2009; Corbelli et al. 2010). Their relative contributions to the mass at distances of interest turn out to be negligible and we do not discuss them in what follows.

[10] We thank A. Kusenko and M. Loewenstein in drawing our attention to these works (Kusenko & Loewenstein 2010).

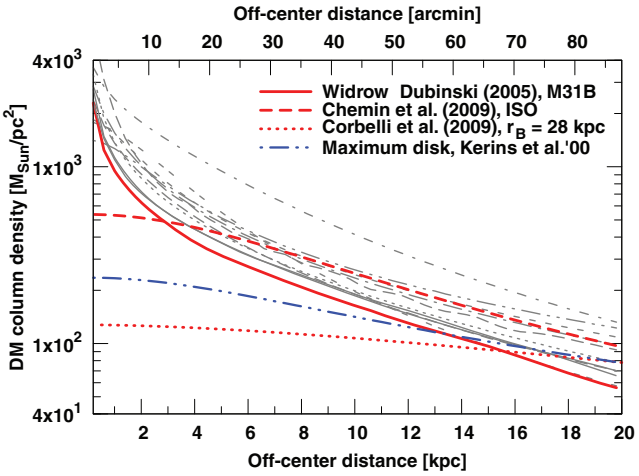

Figure 2. Dark matter column density of M31 as a function of off-centre distance. The grey lines represent models from Kerins et al. (2001), Klypin et al. (2002), Kerins (2004), Widrow & Dubinski (2005), Geehan et al. (2006), Tempel et al. (2007) analysed in B08. The red solid line represents the most conservative model M31B of Widrow & Dubinski (2005). The model of Chemin et al. (2009) (red dashed line), the maximum disc model of Kerins (2004) (blue dashed double-dotted line) and the 'minimal' model of Corbelli et al. (2010) (red dotted line) (see the text) are shown for comparison.

synthesis models (Bell et al. 2003) $\Upsilon_{\rm disc} \simeq 1.7\Upsilon_\odot$ (in agreement with those of Widrow & Dubinski 2005; Geehan et al. 2006). Aiming to reproduce the data in the inner several kpc, they explored different disc-bulge decompositions with two values of the bulge's mass-to-light ratio $\Upsilon_{\rm bulge} \simeq 0.8\Upsilon_\odot$ and $\Upsilon_{\rm bulge} \simeq 2.2\Upsilon_\odot$ (all mass-to-light ratios are in solar units). Chemin et al. (2009) analysed several DM density profiles (NFW, Einasto, cored profile). According to their six best-fitting models (3 DM density profiles times two choices of mass-to-light ratio) the DM column density in the Andromeda galaxy is higher than the one, adapted in B08 (model M31B) everywhere but inside the inner 1 kpc (see red dashed line in Fig. 2).

Corbelli et al. (2010) used circular velocity data, inferred from the H I rotation curves, also extending out to ∼37 kpc. The authors exclude from the analysis the inner 8 kpc, noticing the presence of structures in the inner region (such as a bar), associated with non-circular motions. Corbelli et al. (2010) also use optical data of Walterbos & Kennicutt (1988) and determine an upper and lower bounds on the disc mass-to-light ratio using the same models (Bell & de Jong 2001; Bell et al. 2003) as Chemin et al. (2009). They obtain possible range of values of the *B*-band mass-to-light ratio $2.5\Upsilon_\odot \leq \Upsilon_{\rm disc} \leq 8\Upsilon_\odot$. These values do not take into account corrections for the internal extinction.[11] Corbelli et al. (2010) fit the values of $\Upsilon_{\rm disc}$ rather than fixing it to a theoretically preferred value. The mass-to-light ratio of the disc of a spiral galaxy is known to be poorly constrained in such a procedure since the contributions of the disc and DM halo are similar (see e.g. discussions in Widrow & Dubinski 2005; Chemin et al. 2009). Corbelli et al. (2010) analysed variety of DM models and mass-to-light ratios, providing good fit to the data. The mass model that maximizes the contribution of the stellar disc ($\Upsilon_{\rm disc} = 8$) has the core of the Burkert profile (Burkert 1995) $r_B = 28$ kpc (if one imposes additional constraint on the total mass of M31 within several hundred kpc). The DM column density remains in this model remains essentially flat from the distance $\sim r_B$ inwards (see Fig. 2). Note that the 'maximum disc' fitting of Kerins (2004) (blue dashed double-dotted line in Fig. 2) has higher DM content. Therefore in this work, we will adopt the Burkert DM model of Corbelli et al. (2010) as a *minimal* possible amount of DM, consistent with the rotation curve data on M31. The corresponding DM column density is factor 2–3 lower than the one given by the previously adapted model M31B in the inner 10 kpc. In what follows we will provide the restrictions for both M31B (as the *most conservative* among physically motivated models of DM distribution in M31) and Burkert model of Corbelli et al. (2010).

[11] The correction for foreground extinction was taken into account in Corbelli et al. (2010), using the results of Seigar, Barth & Bullock (2008). The uniform disc extinction was not applied (which explains high values of $\Upsilon_{\rm disc}$). The authors of Corbelli et al. (2010) had chosen not to include any uniform extinction corrections due to the presence of a gradient of *B*-*R* index (Corbelli, private communication).

Table 2. Cleaned exposures and FOV after the removal of point sources and OOT events (calculated using BACKSCAL keyword) of three M31on observations.

ObsID	Cleaned exposure (ks) (MOS1/MOS2/PN)	FOV (arcmin^2) (MOS1/MOS2/PN)
0109270101	16.8/16.7/15.3	335.4/ 336.0/283.6
0112570101	39.8/40.0/36.0	332.9/ 333.1/285.9
0112570401	29.8/29.9/23.5	335.6/336.1/289.5

4.2 M31 central part

Three observations of the central part of M31 (ObsIDs 0112570401, 0109270101 and 0112570101) were used in B08 to search for a DM decay signal. After the removal of bright point sources, the diffuse spectrum was extracted from a ring with inner and outer radii 5 and 13 arcmin, centred on M31[12] (see B08 for details, where this region was referred to as ring 5-13). We call these three observations collectively M31on in what follows. The baseline power-law model has the total χ^2 1328 for 1363 degrees of freedom (d.o.f.; reduced $\chi^2 = 0.974$).

Let us estimate the improvement of the S/N (2), assuming the DM origin of LK10 spectral feature. The average DM column density in the model M31B of Widrow & Dubinski 2005) is $\mathcal{S}_{\rm M31on} = 606\,{\rm M}_\odot\,{\rm pc}^{-2}$. The DM column density from the Milky Way halo in this direction is $74.1\,{\rm M}_\odot\,{\rm pc}^{-2}$.

The ratio of $t_{\rm exp} \times \Omega_{\rm fov} \times A_{\rm eff}$ of all observations of M31on (Table 2) and the LK10 observation is 12.9. Thus one expects the following improvement of the S/N:

$$\frac{({\rm S/N})_{\rm M31on}}{({\rm S/N})_{\rm W1}} = \frac{606+74.1}{208.5+73.9}\sqrt{12.90} \approx 8.65\,, \qquad (4)$$

i.e. the $\sim 2.5\sigma$ signal of LK10 should become a prominent feature (formally about $\sim 21.6\sigma$ above the background) for the M31on observations. As described in Section 3 we add to the baseline power-law spectrum a narrow Gaussian line with the normalization fixed at $F_{\rm M31on} = \frac{606+74.1}{208.5+73.9} F_{\rm W1} \approx 1.08 \times 10^{-7}$ photons cm^{-2} s^{-1} arcmin^{-2}. The quality of fit becomes significantly worse (see Fig. 3). The increase of the total χ^2 due to the adding of a line is equal to $(23.2)^2$, $(22.9)^2$ and $(22.2)^2$ for $1\sigma, 2\sigma$ and 3σ intervals with respect to the central, respectively.

[12] We adopt the distance to M31 $D_{\rm L} = 784$ kpc (Stanek & Garnavich 1998) (at this distance 1 arcmin corresponds to 0.23 kpc).

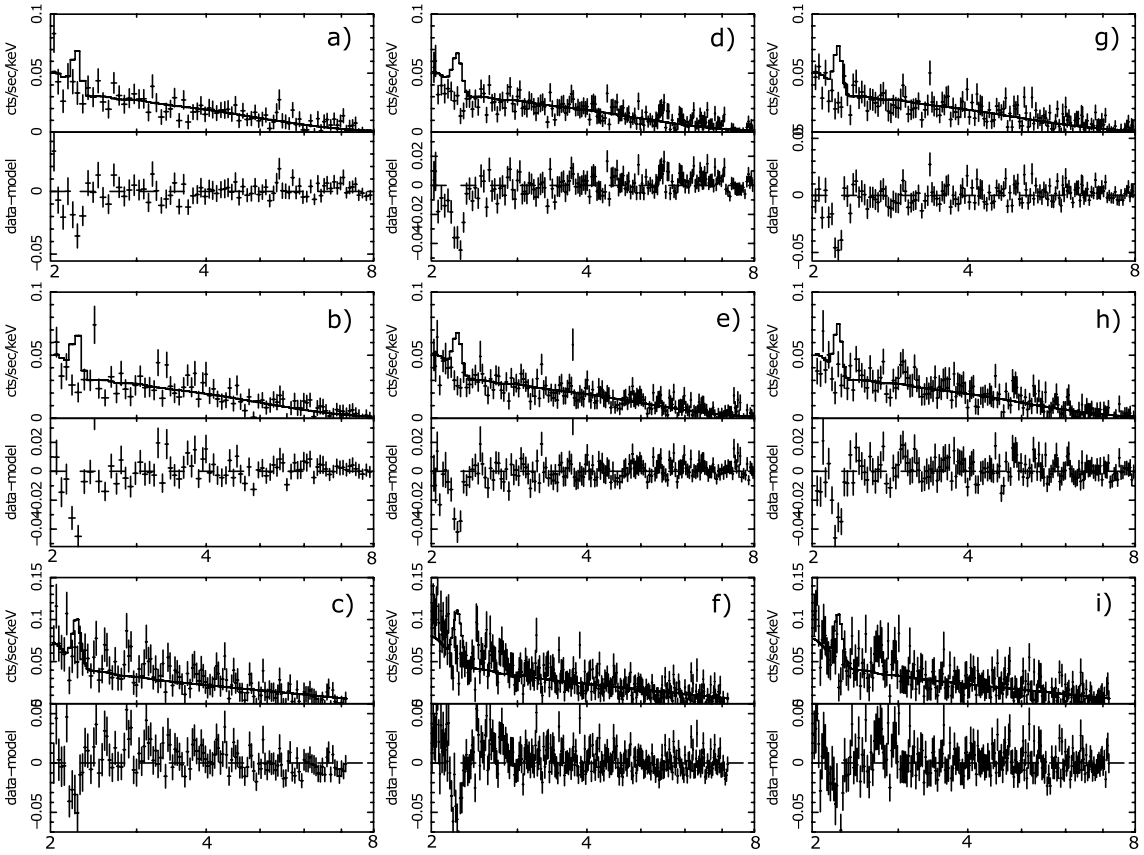

Figure 3. Spectra of three *XMM–Newton* observations of M31 (M31on, Section 4.2). The Gaussian line, obtained by proper scaling of the result of LK10 is also shown. The top row is for MOS1, the middle row for MOS2 and the bottom row for PN cameras. The spectra in the left-hand column are for the observation 0109270101, the middle column for 0112570101 and the right-hand column for 0112570401. The error bars include 5 per cent of the model flux as an additional systematic error. For all these spectra combined together, the χ^2 increases by *at least* 22.2^2, when adding a narrow Gaussian line in any position between 2.3 and 2.72 keV (see the text).

Table 3. Cleaned exposures and FOV (calculated using BACKSCAL keyword) of the observation M31off (ObsID 0402560301). The significant difference in FOVs between MOS1 and MOS2 cameras is due to the loss CCD6 in MOS1 camera.

ObsID	Cleaned exposure (ks) (MOS1/MOS2/PN)	FOV (arcmin^2) (MOS1/MOS2/PN)
0402560301	41.9/42.2/35.2	405.6/ 495.4/433.3

In addition to the M31on observations, we processed an *XMM–Newton* observation 0402560301, positioned ≈22 arcmin off-centre M31 (RA = $00^h40^m47\overset{s}{.}64$, Dec. = $+41^d18^m46\overset{s}{.}3$) – M31off observation, see Table 3. We collected the spectra from the central 13 arcmin circle. Several point sources were manually excluded from the source spectra. The rest of data reduction is described in the Section 4.2. The fit by the power-law model is excellent, the total χ^2 equals to 895 for 997 d.o.f. (the reduced $\chi^2 = 0.898$). Using the DM estimate based on the model M31B we find that the average DM column density for the M31off $\mathcal{S}_{\rm M31off} = 388.6\,{\rm M}_\odot\,{\rm pc}^{-2}$ plus the Milky Way halo contribution $74.3\,{\rm M}_\odot\,{\rm pc}^{-2}$. The estimate of the line significance is similar to the previous section and gives

$$\frac{({\rm S/N})_{\rm M31off}}{({\rm S/N})_{\rm W1}} = \frac{388.6+74.3}{208.5+73.9}\sqrt{8.76} \approx 4.85 \qquad (5)$$

and therefore under the assumption of DM nature of the feature of LK10, one would expect $\sim 12.1\sigma$ detection. After that, we add a narrow line with the normalization $F_{\rm M31off} \approx 7.37 \times 10^{-8}$ photons cm^{-2} s^{-1} arcmin^{-2} and perform the procedure, described in Section 3. The observation M31off rules out the DM decay line origin of the LK10 feature with high significance (see Fig. 4): the increase of χ^2 due to the addition of this line has the minimum value $\Delta\chi^2 \simeq (10.4)^2$ at 2.44 keV, which is within 1σ interval of the quoted central value of the LK10 feature.

We also perform the analysis, adding a line, whose flux is determined according to the DM density estimates based on the model of Corbelli et al. (2010), that we consider to be a minimal DM model for M31 (as discussed in Section 4.1). For this model the column density in the central 1–3 kpc decreases by a factor of ∼3.4 as compared with the value, based on M31B. Kusenko & Loewenstein (2010) claimed that in this case the LK10 line becomes consistent with the M31on observations. However, our analysis shows that the total χ^2 *increases*, when adding the corresponding line to the model, by $(5.7)^2$ for 3σ variation of the position of the line. The corresponding increase of total χ^2 for M31off region is $(2.0)^2$. Combining M31on and M31off observations, one obtains $(6.2)^2$ increase of the total χ^2.

We conclude therefore that despite the uncertainties in DM modelling, the analysis of diffuse emission from the central part of M31 (1–8 kpc off the centre), as measured by *XMM–Newton*, disfavours the hypothesis that the spectral feature, observed in Willman 1, is due to decaying DM. Nevertheless, to strengthen this conclusion further we analysed available *XMM–Newton* observations of M31

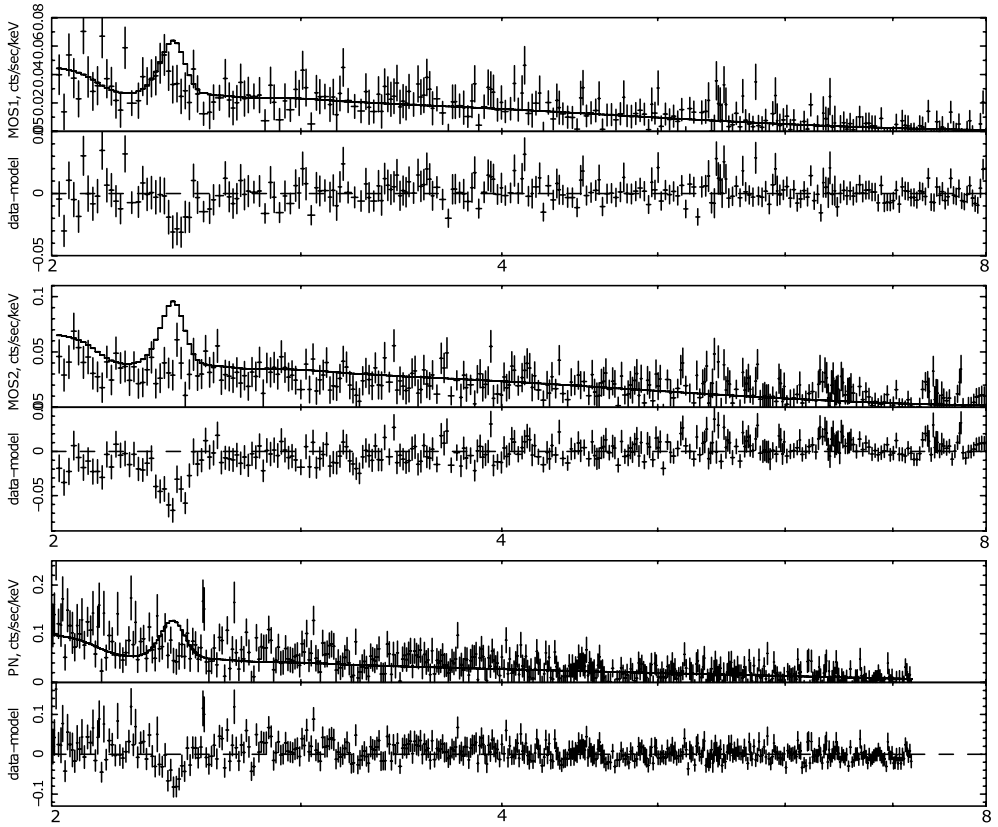

Figure 4. The spectra of off-centre M31 observation 0402560301 (M31off, Section 4.3). The decaying dark matter signal, obtained by proper scaling of the result of LK10 is also shown. The error bars include 5 per cent of the model flux as an additional systematic error. Fitting these spectra together excludes the properly scaled line of LK10, at the level of at least 10.4σ (see the text).

Table 4. Cleaned exposures and FOV after the removal of point sources and OOT events (calculated using BACKSCAL keyword) of nine M31 observations offset by more than 10 kpc from the centre (M31out observations).

ObsID	Cleaned exposure (ks) (MOS1/MOS2/PN)	FOV (arcmin^2) (MOS1/MOS2/PN)
0511380101	44.3/44.5/37.6	356.2/400.4/333.3
0109270401	38.5/38.4/33.5	387.8/384.1/366.7
0505760401	26.0/26.0/21.7	330.5/374.1/325.0
0505760501	23.8/23.8/19.8	344.8/395.2/313.2
0402561301	22.7/22.7/20.1	367.2/419.5/382.6
0402561401	39.3/39.3/33.7	349.9/408.3/343.6
0402560801	42.6/42.6/36.6	373.6/435.8/393.7
0402561501	38.5/38.5/34.0	369.3/421.0/407.5
0109270301	24.4/24.6/22.2	443.4/439.6/405.0

in the region 10–20 kpc off-centre, where the uncertainties in the mass modelling of M31 reduce significantly as compared with the central 5–8 kpc (cf. Chemin et al. 2009; Corbelli et al. 2010, see also Section 4.1, in particular Fig. 2).

4.3 M31 off-centre (10–20 kpc)

We selected nine observations with MOS cleaned exposure greater than 20 ks (Table 4). The total exposure of these observations is about 300 ks. Based on the statistics of these observations one would expect a detection of the signal of LK10 with the significance 12.1σ (for M31B) and 11.2σ (for Corbelli et al. 2010). The fit to the baseline model is very good, giving total χ^2 equal to 5931 for 5883 d.o.f. (the reduced $\chi^2 = 1.008$). However, adding the properly rescaled line significantly reduced the fit quality, increasing the total χ^2 by $(12.0)^2/(10.7)^2/(10.7)^2$ when varying line position within $1\sigma, 2\sigma$ and 3σ intervals (using M31B model) and by $(11.7)^2$, $(10.7)^2$ and $(10.6)^2$ for $1\sigma, 2\sigma$ and 3σ intervals [using the model of Corbelli et al. (2010), which gives DM column density in M31out about 160–180 $M_\odot$ pc^{-2} (including Milky Way contribution), see Fig. 2].

4.4 Combined exclusion from M31

Finally, performing a combined fit to all 13 observations of M31 (M31, M31off, M31out) we obtain the exclusion of more than 26σ (using the DM model M31B of Widrow & Dubinski 2005) and more than 13σ for the minimal DM model of Corbelli et al. (2010). As described in Section 3, in deriving these results we allowed the normalization of the baseline power-law model to vary independently for each camera, observing the same spatial region, added additional 5 per cent of the model flux as a systematic uncertainty and allowed the position of the narrow line to vary within 2.3–2.72 keV interval.

5 DWARF SPHEROIDAL GALAXIES

Since Willman 1 is purported to be a dwarf spheroidal (dSph) galaxy (but see Section 5.1), as the next step in examining the hypothesis of LK10 we compare estimates of the dark mass of Willman 1 to dark masses estimated for other dSph satellites of the Milky Way.

Specifically we consider two of the (optically) brightest dSphs, Fornax and Sculptor, for which comparable X-ray data exist. To characterize the DM haloes of dSphs, we adopt the general DM halo model of Walker et al. (2009a), with density profile given by

$$\rho(r) = \rho_{\rm s}\left(\frac{r}{r_{\rm s}}\right)^{-\gamma}\left[1+\left(\frac{r}{r_{\rm s}}\right)^{\alpha}\right]^{\frac{\gamma-3}{\alpha}}, \quad (6)$$

where the parameter α controls the sharpness of the transition from inner slope $\lim_{r\to 0}$ d ln (ρ)/d ln $(r) \propto -\gamma$ to outer slope $\lim_{r\to\infty}$ dln (ρ)/d ln $(r) \propto -3$. This model includes as special cases both *cored* ($\alpha = 1$, $\gamma = 0$) and NFW (Navarro et al. 1997) ($\alpha = \gamma = 1$) profiles. Assuming that dSph stars are spherically distributed as massless test particles tracing the DM potential, the DM density relates to observables – the projected stellar density and velocity dispersion profiles – via the Jeans Equation (see equation 3 of Walker et al. 2009a). Walker et al. (2009a) show that while the data for a given dSph do not uniquely specify any of the halo parameters individually, the bulk mass enclosed within the optical radius is generally well constrained, subject to the validity of the assumptions of spherical symmetry and dynamic equilibrium and negligible contamination of stellar velocity samples from unresolved binary-orbital motions.

5.1 Willman 1

Despite some indications that Willman 1 is a dark-matter dominated dSph galaxy (Martin et al. 2007; Strigari et al. 2008), it should be noted that the galactic status of Willman 1 remains uncertain. Claims that Willman 1 is a *bona fide* galaxy – as opposed to a star cluster devoid of DM – stem primarily from two considerations. First, under simple dynamical models, the stellar velocity dispersion (4.3 ± 2.5 km s^{-1}; Martin et al. 2007) of Willman 1 implies a large mass-to-light ratio ($M/L_V \sim 700\,{\rm M}_\odot/{\rm L}_{V,\odot}$), indicative of a dominant DM component like those that characterize other dSph galaxies. Second, the initial spectroscopic study by Martin et al. (2007) suggests that Willman 1 stars have a metallicity range $-2.0 \leq$ [Fe/H] ≤ -1.0, significantly broader than is observed in typical star clusters. However, both arguments are vulnerable to scrutiny. For example, if the measured velocity dispersion of Willman 1 receives a significant contribution from unresolved binary stars and/or tidal heating, then the inferred mass may be significantly overestimated. Demonstrations that binary orbital motions contribute negligibly to dSph velocity dispersions have thus far been limited to intrinsically 'hotter' systems, with velocity dispersions $\sigma_V \sim 10$ km s^{-1} (Olszewski, Aaronson & Hill 1995; Hargreaves, Gilmore & Annan 1996). Furthermore, given Willman 1's low luminosity, kinematic samples must include faint stars close to the main-sequence turnoff (see fig. 8 of Martin et al. 2007). These stars are physically smaller than the bright red giants observed in brighter dSphs, and thus admit tighter, faster binary orbits. Therefore, the degree to which binary motions may inflate the estimated mass of Willman 1 remains unclear. Finally, follow-up spectroscopy by Siegel, Shetrone & Irwin (2008) suggests that the relatively high-metallicity stars observed by Martin et al. (2007) are in fact foreground contaminants contributed by the Milky Way along the line of sight to Willman 1. Removal of these stars from the sample would erase the large metallicity spread reported by Martin, de Jong & Rix (2008), and the remaining stars would have a narrow metallicity distribution consistent with that of a *metal-poor globular cluster* (Siegel et al. 2008). Nevertheless, we proceed under the assumption that Willman 1 is indeed a dSph galaxy for which the measured stellar velocity dispersion provides a clean estimate of the DM content. This assumption gives conservative estimates of the expected DM decay signal in other objects (including M31), since any overestimate of the DM column density in Willman 1 will result in an underestimate of the relative S/N expected in other objects (see equation 2). For Willman 1 we adopt the line-of-sight velocity data for 14 member stars observed by Martin et al. (2007). These stars, which lie a mean distance of 30 pc in projection from the centre of Willman 1, have a velocity dispersion of $\sigma_V = 4.3 \pm 2.5$ km s^{-1}. To specify the stellar surface density, we adopt a Plummer profile, $I(R) = I_0[1 + R^2/r_{\rm half}^2]^{-2}$, with parameters $r_{\rm half} = 25$ pc and $I_0 = 0.5\,{\rm L}_\odot\,{\rm pc}^{-2}$ as measured by Martin et al. (2008). Of course the single point in the empirical velocity dispersion 'profile' relates no information about the *shape* of the profile, and these data therefore provide only weak constraints on the DM content of Willman 1. The solid black line in the bottom-left panel of Fig. 5 displays the median spherically enclosed mass profile for the general halo model of equation (6), with dotted lines enclosing the region corresponding to the central 68 per cent of posterior parameter space from the Markov chain Monte Carlo analysis (see Walker et al. (2009a) for a detailed description of the MCMC procedure). The small published kinematic data set (14 stars) for Willman 1 allows for only a single bin in the velocity dispersion profile [see the upper right-hand panel in Fig. 5 and compare it e.g. with Fornax dSph (the left-hand panel)]. This resulting constraints on the mass profile of Willman 1 are therefore very poor. The allowed masses *span several orders of magnitude at all radii of interest* and are consistent with negligible DM content – the lower bound (68 per cent confidence interval) on the mass within 200 pc (including all of the Willman 1) is as low as $100\,{\rm M}_\odot$. Strigari et al. (2008) obtained for Willman 1 $M(<100\,{\rm pc}) = 1.3^{+1.5}_{-0.8} \times 10^6\,{\rm M}_\odot$ with the DM column density for the best-fitting values of parameters being $\mathcal{S}_{\rm W1} \sim 200\,{\rm M}_\odot\,{\rm pc}^{-2}$. The discrepancy with results of Strigari et al. (2008) may arise from two possible sources. First, Strigari et al. (2008) use an independent, still unpublished kinematic data set (Willman et al., in preparation) for Willman 1. Although the global velocity dispersion is statistically equivalent to that which we measure from Martin et al. (2008) sample, the data set used by Strigari et al. (2008) is larger, containing 47 Willman 1 members. Secondly, Strigari et al. (2008) adopt more stringent priors motivated by cosmological N-body simulations, under which $\rho_{\rm s}$ and $r_{\rm s}$ are strongly correlated (Bullock & Johnston 2007; Diemand, Kuhlen & Madau 2007). We have used more general models here in order to help illustrate the uncertainties in the mass modelling of Willman 1. However, in the interest of obtaining the most conservative estimates for the signal we expect to see from other objects if the LK10 detection is real, we shall continue to adopt one of the largest available estimates of the DM column density in Willman 1 – namely, the value of $\mathcal{S}_{\rm W1} = 208.5\,{\rm M}_\odot\,{\rm pc}^{-2}$ that results from the modelling of Strigari et al. (2008).

5.2 Fornax and Sculptor dSphs

For Fornax and Sculptor, two of the brightest and most well-studied dSph satellites of the Milky Way, the availability of large kinematic data sets of ∼2600 and ∼1400 members, respectively (Walker, Mateo & Olszewski 2009b), allows us to place relatively tight constraints on the DM column densities. Fig. 5 displays the empirical velocity dispersion profiles, as well as the fits we obtain from the general (equation 6), NFW and cored halo models. Adopting a Fornax distance of ∼138 kpc (Mateo 1998), we integrate the projected density profile out to a radius of 560 pc, which

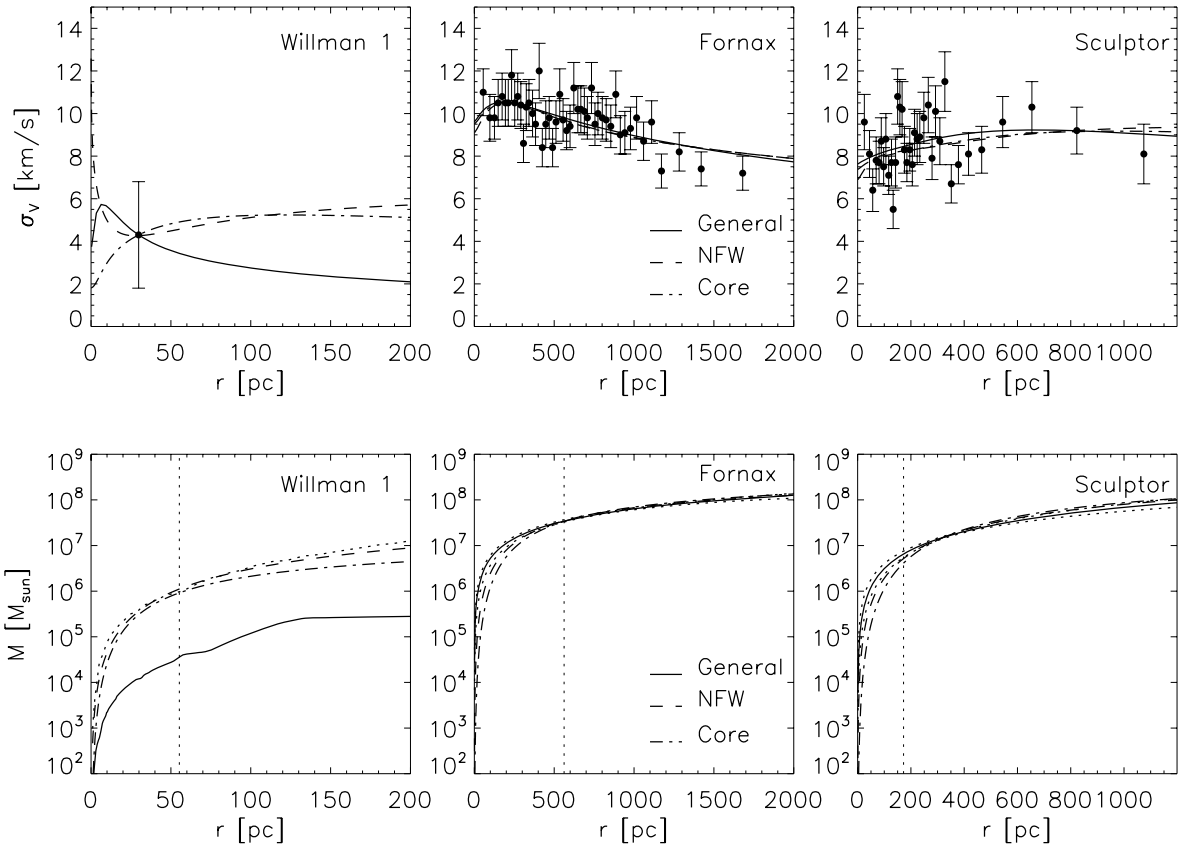

Figure 5. DM mass modelling in Fornax and Willman 1. Top panels display empirical velocity dispersion profiles as calculated by Walker et al. (2009a) for Fornax, Sculptor and from the Willman 1 data of Martin et al. (2007) (for Willman 1, the small published sample of 14 stars allows for only a single bin). Overplotted are the median profiles obtained from the MCMC analysis described by Walker et al. (2009a), using the general dark matter halo model (6), as well as the best-fitting NFW and cored halo models. Bottom panels indicate the corresponding spherically-enclosed mass profiles. In the bottom panels, dashed lines enclose the central 68 per cent of accepted general models (for Willman 1, the lower bound falls outside the plotting window). Vertical dotted lines indicate the outer radius of the FOV of the X-ray observations (14 arcmin for Fornax, 7.5 arcmin for Sculptor and 5 arcmin for Willman 1).

Table 5. Best-fitting NFW ($\alpha = \gamma = 1$ in equation 6) and core profiles ($\alpha = 1, \gamma = 0$) for Fornax and Sculptor dSphs

	Fornax		Sculptor	
	ρ_s ($M_\odot$ pc^{-3})	r_s	ρ_s ($M_\odot$ pc^{-3})	r_s
NFW	0.1	500	0.04	920
Core	0.57	280	0.48	350

corresponds to the 14 arcmin region (extraction region of *XMM–Newton* observation, see below) and is similar to the half-light radius of Fornax. For Fornax, the best-fitting density profile parameters are given in Table 5.[13] For NFW density profile ($V_{max} = 17.0\,km\,s^{-1}$) gives $\mathcal{S}_{Forn,NFW} = 55.2\,M_\odot\,pc^{-2}$ and the best-fitting cored profile ($V_{max} = 17.4\,km\,s^{-1}$) gives a slightly lower value $\mathcal{S}_{Forn} = 54.4\,M_\odot\,pc^{-2}$ that we adopt for subsequent analysis.

Adopting a Sculptor distance of 79 kpc (Mateo 1998), we integrate the projected density profile over a square of 175^2 pc^2, which corresponds to the 7.6 arcmin^2 region (extraction region of *Chandra* observations on the ACIS-S3 chip, see below). The best-fitting parameters for Sculptor are given in Table 5. The best-fitting cored profile ($V_{max} = 19.8\,km\,s^{-1}$) gives a DM column density $\mathcal{S}_{Scul,core} = 147\,M_\odot\,pc^{-2}$ and the best-fitting NFW profile ($V_{max} = 19.4\,km\,s^{-1}$), gives $\mathcal{S}_{Scul,NFW} = 140.3\,M_\odot\,pc^{-2}$ and that we adopt for subsequent analysis. Notice that using the parameters of the 'universal DM density profile' of Walker et al. (2009a), one would get only slightly higher values. In any case, the DM column densities of Fornax and Sculptor are much more tightly constrained than that of Willman 1. The Fornax column density is smaller than the expected column density of Milky Way halo in the direction of Fornax, which we estimate to be $83.2\,M_\odot\,pc^{-2}$. The estimated DM column density of the Milky Way in the direction of Sculptor is $95.7\,M_\odot\,pc^{-2}$ (see Section 2).

5.3 *XMM–Newton* observation of Fornax dSph

Fornax is one of the most deeply observed dSphs in X-ray wavelengths. We have processed the 100 ks *XMM–Newton* observation (ObsID 0302500101) of the central part of Fornax dSph. The data analysis is described in the Section 3. In each camera, we extract signal from the 14 arcmin circle, centred on the Fornax dSph. The cleaned exposure and corresponding fields of view (calculated using the BACKSCAL keyword) for all three cameras (after subtraction

[13] Note that the fitting parameters ρ_s and r_s are typically degenerate in the mass modelling of dSphs (Strigari et al. 2006; Peñarrubia, McConnachie & Navarro 2008). Thus neither parameter is constrained uniquely. The best fits considered here generally represent a 'family' of models that follow a ρ_s, r_s relation consistent with the data, but which all tend to have the same bulk mass enclosed within the optical radius (Peñarrubia et al. 2009).

Table 6. Cleaned exposures of the *XMM–Newton* observation of Fornax dSph

XMM–Newton ObsID	Cleaned exposure (ks) (MOS1/MOS2/PN)	FOV (arcmin^2) (MOS1/MOS2/PN)
0302500101	53.8/53.9/48.2	459.1/548.5/424.9

of CCD gaps, OOT strings in PN camera and CCD 6 in MOS1 camera) are shown in Table 6. Based on the DM estimates, presented in the Section 5.2 we expect the following improvement in S/N:

$$\frac{(\mathrm{S/N})_{\mathrm{Forn}}}{(\mathrm{S/N})_{\mathrm{W1}}} = \frac{54.4 + 83.2}{208.5 + 73.9}\sqrt{12.12} \approx 1.70, \quad (7)$$

i.e. we expect a $\sim 4.2\sigma$ signal from Fornax, assuming DM decay line origin of the LK10 feature.

The fit to the baseline model is very good, $\chi^2 = 955$ for 983 d.o.f. (reduced $\chi^2 = 0.972$). Note that the parameters are consistent with those of extragalactic diffuse X-ray background as it should be for the dwarf spheroidal galaxy where we do not expect any diffuse emission at energies above 2 keV (see also Boyarsky et al. 2006b, 2007b; Jeltema & Profumo 2008; Loewenstein et al. 2009; Riemer-Sorensen & Hansen 2009).

After adding a narrow line with the normalization $F_{\mathrm{Forn}} \approx 2.19 \times 10^{-8}$ photons cm^{-2} s^{-1} arcmin^{-2}, the χ^2 *increases*, the minimal increase is equal to $(5.1)^2$, $(4.2)^2$ and $(3.3\sigma)^2$ for a position of the line within 1σ, 2σ and 3σ intervals from LK10 feature, respectively (after adding 5 per cent of model flux as a systematic error). We see that adding a properly scaled Gaussian line worsens χ^2 by at least $\sim 3.3\sigma$ (instead of expected *improvement* of the quality of fit by a factor of about 16 if the LK10 feature were the DM decay line), see Fig. 6 for details.

The combination of all *XMM–Newton* observations used in this work (M31on, M31off, M31out and Fornax) provide a minimum of 26.7σ exclusion at 2.35 keV (which falls into the 3σ energy range for the LK10 spectral features), after adding a 5 per cent systematic error. Within 1σ and 2σ energy intervals, the minimal increase of χ^2 is 29.0^2 and 27.3^2, correspondingly. Therefore, one can exclude the DM origin of the LK10 spectral feature by 26σ. This exclusion is produced by using the most conservative DM model M31B of Widrow & Dubinski (2005). Using the minimal DM model of Corbelli et al. (2010), one can exclude the LK10 feature at the level more than 14σ.

5.4 *Chandra* observations of the Sculptor dSph

5.4.1 The data and data preparation

For the Sculptor dSph there is one observation of 50 ks (ObsId 9555) and 21 observations of 5–6 ks (ObsID 4698–4718), see Table 7 for details. In all the observations, the centre of Sculptor is on the ACIS-S3 chip, and we have restricted the analysis to this chip.

Throughout the entire analysis we used CIAO 4.1 with CALDB 4.1 (Fruscione et al. 2006) and XSPEC 12.4 (Arnaud, Dorman & Gordon 2009). All the data were observed using the VFAINT telemetry mode and thus required reprocessing prior to any data analysis in order to take advantage of the improved background event rejection based on 5×5 pixel islands instead of the normal 3×3 pixel.

We used the wavelet algorithm *wavdetect* in CIAO to find and exclude point sources for each observation. The removed areas are very small compared to the FOV, and were consequently neglected in the following analysis. Furthermore the observations were light-curve cleaned using *lc_clean*. The observations 4705 and 4712 were flared and left out in the subsequent analysis. The number of point sources removed and the exposure time after light-curve cleaning are given in Table 7. The variation in the number of point sources is mainly due to slightly different observed areas. The observations are all centred on the same spot, but there is a variation in detector roll angles. Assuming spherical symmetry of Sculptor, this has no importance for the further analysis.

5.4.2 The spectra

The spectra were extracted from a square region of 7.6×7.6 arcmin^2 covering most of the ACIS-S3 chip but excluding the edges where the calibration is less precise (*Chandra* X-ray Centre 2009). For later fitting they where binned to at least 15 counts per bin.

The spectra of the short observations (4698–4718, except 4705, 4712) were combined into one observation, see Fig. 7. This is justified because they fulfil the following criteria: They are observations of the same (non-variable) object and thus have similar count rates, they are extracted from the same region of the same chip, their response matrix functions (rmfs) are extremely similar. The spectra were added using the FTOOL *mathpha* (Irby 2008) with the uncertainties propagated as if they were pure Gaussian.

5.4.3 Background subtraction

We subtracted only the particle background as observed with the ACIS detector stowed.[14] Around 2005 there was a change in the spectral shape of ACIS-S3 and consequently new particle background files were produced (Markevitch 2009). We used the new particle background files (2005–2009) for both spectra. The particle background was normalized in the 10–12 keV interval where any continuous emission from Sculptor is negligible (Markevitch et al. 2003). For 9555 the effect of changing the normalization interval to e.g. 4–6 keV is less than 3 per cent. For the combined observations there is a larger excess at low energies, which makes it more sensitive to the choice of normalization interval and consequently we chose the conservative approach with the 10–12 keV interval. The larger excess might come from point sources, which are unresolved in the short exposures, but resolved and thus removed in the long exposure. The excess is mainly at energies below 2 keV and are irrelevant to the present analysis.

The background subtracted spectra are shown in Fig. 7 with the combined observations in black and ObsID 9555 in a lighter (green) colour. Also shown is the best fit to a power-law model and the Gaussian expected according to the signal proposed by LK10 which is further discussed below.

5.4.4 Constraints

The total exposure of Sculptor is 162.1 ks which is 1.63 times longer than the Willman 1 observation. Sculptor is observed with the ACIS-S3 chip, which at 2.5 keV has an effective area that is 1.23 times larger than that of ACIS-I which Willman 1 is observed with. The Sculptor spectra are extracted from a $(7.6\,\mathrm{arcmin})^2$ square, which is 0.74 of the 5 arcmin circle for which the Willman 1 spectra were extracted.

$$\frac{(\mathrm{S/N})_{\mathrm{Sc}}}{(\mathrm{S/N})_{\mathrm{W1}}} = \frac{140.3 + 95.7}{208.5 + 73.9}\sqrt{1.63 \times 1.23 \times 0.74} = 1.02, \quad (8)$$

[14] The files can be downloaded from http://cxc.harvard.edu/contrib/maxim/acisbg/.

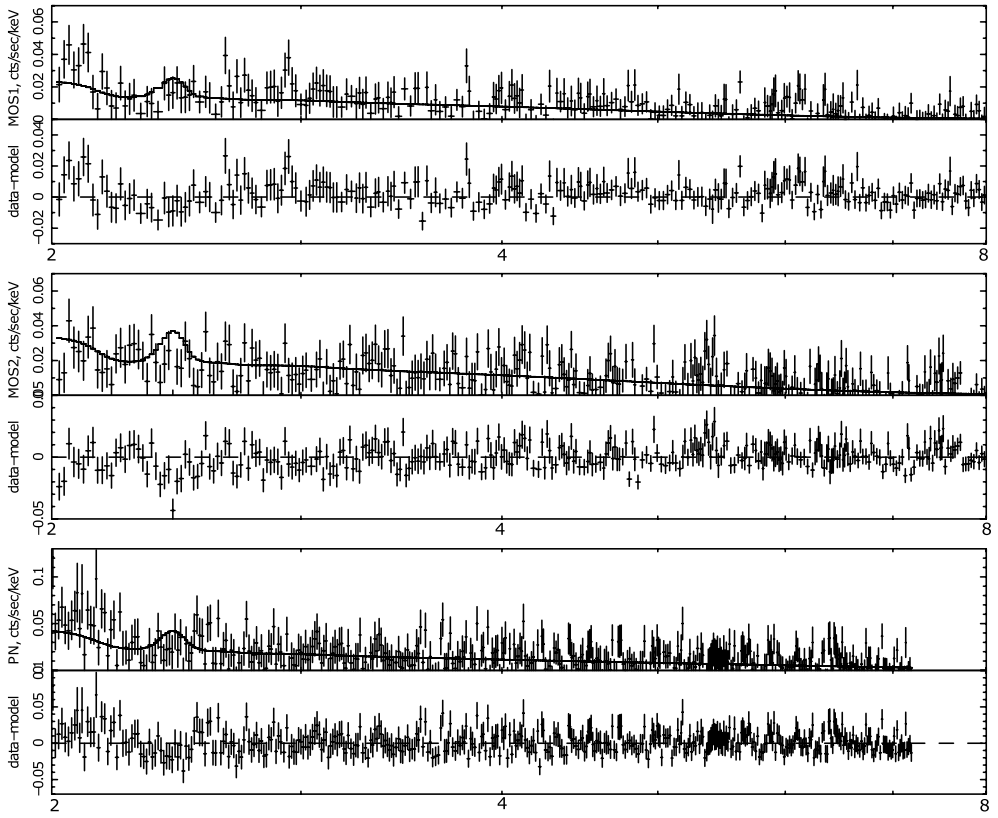

Figure 6. The spectra of the *XMM–Newton* observation 0302500101, Section 5.2. The error bars include 5 per cent of the model flux as an additional systematic error. Fitting these spectra together excludes the properly scaled LK10 line at the level of at least 2σ (3.3σ if one restricts the position of the line to the interval 2.30–2.72 keV) instead of expected improving of the quality of fit by about 4σ (if the line were of the DM origin).

Table 7. The analysed *Chandra* observations of Sculptor Dwarf.

ObsID	Obs date	Exposure (s)[a]	Point sources[b]
4698	2004 Apr 26	6060	9
4699	2004 May 7	6208	6
4700	2004 May 17	6104	8
4701	2004 May 30	6069	8
4702	2004 Jun 12	5883	7
4703	2004 Jun 27	5880	8
4704	2004 Jul 12	5915	9
4705	2004 Jul 24	–	6
4706	2004 Aug 4	6075	8
4707	2004 Aug 17	5883	8
4708	2004 Aug 31	5880	8
4709	2004 Sep 16	6091	10
4710	2004 Oct 1	5883	8
4711	2004 Oct 11	5727	9
4712	2004 Oct 24	–	7
4713	2004 Nov 5	6073	11
4714	2004 Nov 20	5649	13
4715	2004 Dec 5	5286	10
4716	2004 Dec 19	6016	8
4717	2004 Dec 29	6073	11
4718	2005 Jan 10	6060	10
Short obs combined	–	113 169	–
9555	2008 Sep 12	48 935	21
All obs	–	162 104	–

[a]The exposure times after light-curve cleaning using *lc_clean*.
[b]The number point sources found by *wavdetect* and removed.

i.e. we expect a significance of 2.5σ in case of a DM signal similar to the one of LK10.

Fitting a power law to the two spectra simultaneously over the interval 2.1–10 keV gives an index of $1.54^{+0.35}_{-0.18}$ and a normalization of $(1.22^{+0.74}_{-0.29}) \times 10^{-6}$ photons keV^{-1} cm^{-2} arcmin^{-2}. The fit is excellent with $\chi = 1135$ for 1078 d.o.f. (reduced $\chi^2 = 1.05$).

The ratio $(M^{\rm fov}_{\rm DM}/D^2_{\rm L})_{\rm Scu} = 1138\,{\rm M}_\odot/{\rm kpc}^2$ for Sculptor which is only 0.605 of the same ratio for Willman 1 (including the Milky Way contribution in both cases) giving a flux normalization of 2.03×10^{-6} photons cm^{-2} s^{-1}. We add this Gaussian to the power-law model varying the position over the energy interval 2.1–2.8 keV. The quality of the fit *worsen* (instead of expected improvement) with the lowest increase in χ^2 being 1141 at 2.3 keV. At 2.5 keV the increased value is 1144 which allows us to exclude the possibility of a 2.5 keV feature to be a decay line at the level of $\sqrt{1144 - 1135} = 3\sigma$.

6 DISCUSSION

This work provides more than 80 times improvement of statistics of observations, as compared to LK10 (factor of approximately five times larger total exposure time and factor of approximately four improvement in both the effective area and the FOV). Even under the most conservative assumption about the DM column density such an improvement should have led to an about 14σ detection of the DM decay line. In our analysis no significant lines in the position, predicted by LK10 were found. However, in the *XMM–Newton* observations that we processed there are several spectral features in the range 2–3 keV (see Table 8). This is not surprising,

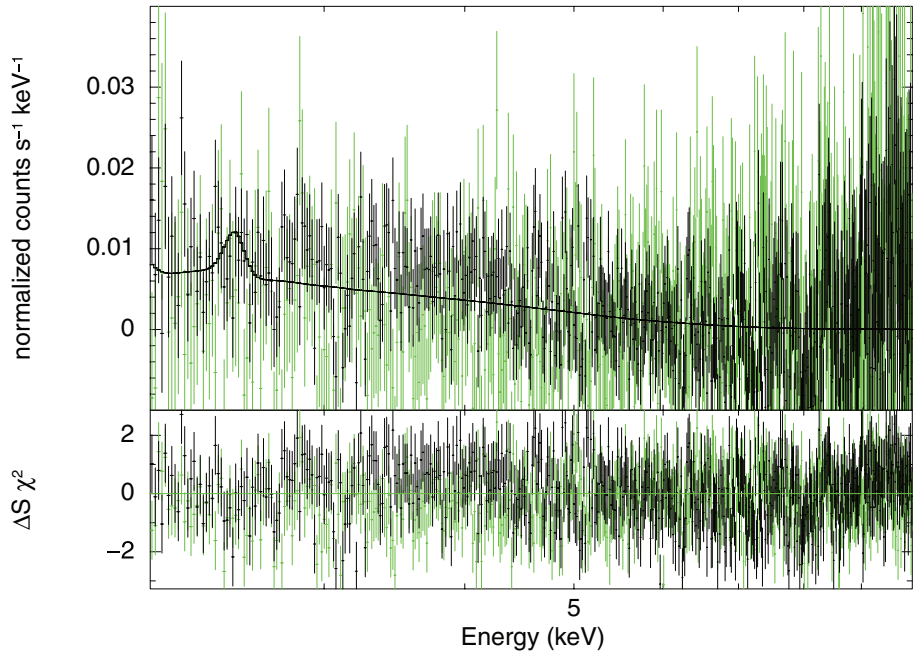

Figure 7. The background subtracted *Chandra* spectra of Sculptor dSph with the short combined observations in black and ObsID 9555 in a lighter (green) colour. Also shown the best-fitting power-law model fitted to both observations simultaneously (index fixed to 1.46) and a Gaussian corresponding to the expected DM line emission as suggested by LK10. The dip in the residuals is a visual indication of the absence of any line signal at ∼2.5 keV.

Table 8. Parameters of the best-fitting power-law components (assuming the power law+Gauss model) and of the maximally allowed flux in the narrow Gaussian line in the interval 2.1–2.8 keV. The slight difference between these values and those of Table 1 is due to the presence of Gaussian component and the proportionality of power law normalization to FOV solid angle (for M31on); for each observation, the corresponding parameters coincide within 90 per cent confidence range. The values of best-fitting power-law parameters for M31out are not shown because they are different for different observations (see Table 1).

Observations	Power-law index, best-fitting value	PL normalization best-fitting value, 10^{-6} ph./(cm^2 s arcmin^2 keV)	Line position (keV)	Significance	Line flux best-fitting value ph./(cm^2 s arcmin^2)	Line flux 3σ upper bound ph./(cm^2 s arcmin^2)
M31on	1.32	1.66/1.82/2.39	2.55	1.7σ	7.35×10^{-9}	2.09×10^{-8}
M31off	1.42	1.51/1.19/2.22	2.47	2.3σ	6.69×10^{-9}	3.10×10^{-8}
M31out	–	–/–/–	2.52	1.6σ	3.76×10^{-9}	1.16×10^{-8}
Fornax	1.37	0.79/0.59/0.70	2.19	2.6σ	9.63×10^{-9}	2.11×10^{-8}

as the *XMM–Newton* gold-coated mirrors have Au absorption edge at ∼2.21 keV (Kirsch et al. 2002, 2004) and therefore their effective areas possess several prominent features in the energy range 2–3 keV. According to *XMM–Newton* calibration report (Kirsch et al. 2002, 2004), there is about 5 per cent uncertainty at the modelling of the effective area of both MOS and PN cameras at these energies. These uncertainties in the effective area can lead to artificial spectral features due to the interaction of the satellite with cosmic rays.[15] In particular, the solar protons with energies of few hundreds keV can be interpreted as X-ray photons (so-called *soft proton flares*). The interaction efficiency of solar protons with the instrument is known to be totally different from that of real photons (Kuntz & Snowden 2008). In particular, their flux is not affected by the Au edge of the *XMM–Newton* mirrors. According to Kuntz & Snowden (2008), the spectrum of soft proton flares for EPIC cameras is well described by the *unfolded* (i.e. assuming that the instrument's response is energy-independent) broken power-law model with the break energy around ∼3.2 keV, bknpow/b in XSPEC v.11. Therefore, modelling the spectrum that is significantly contaminated with soft proton flares in a standard way (i.e. by using *folded* power-law model) will produce artificial residual excess at energies of sharp decreases of the instrument's effective area.

In our data analysis we performed both the standard flare screening (Read & Ponman 2003; Nevalainen et al. 2005; Carter & Read 2007) that uses the inspection of high-energy (10–15 keV) light curve and an additional soft proton flare cleaning. As found by Pradas & Kerp (2005), it is possible to screen out the remaining flares, e.g. by the visual inspection of the cleaned light curve at low and intermediate energies. To provide the additional cleaning after the rejection of proton flares at high energies, we followed the procedure of De Luca & Molendi (2004) and Kuntz & Snowden (2008), leaving only the time intervals, where the total count rate differs from its mean value by less than 2σ.

To test the possible instrumental origin of the features, discussed in this section, we first performed only a high-energy light-curve cleaning (Read & Ponman 2003; Nevalainen et al. 2005; Carter & Read 2007) and determined the maximally allowed flux in a narrow line in the energy interval of interest. After that we performed an additional soft proton cleaning. This procedure improved the quality

[15] See e.g. http://www.star.le.ac.uk/∼amr30/BG/BGTable.html.

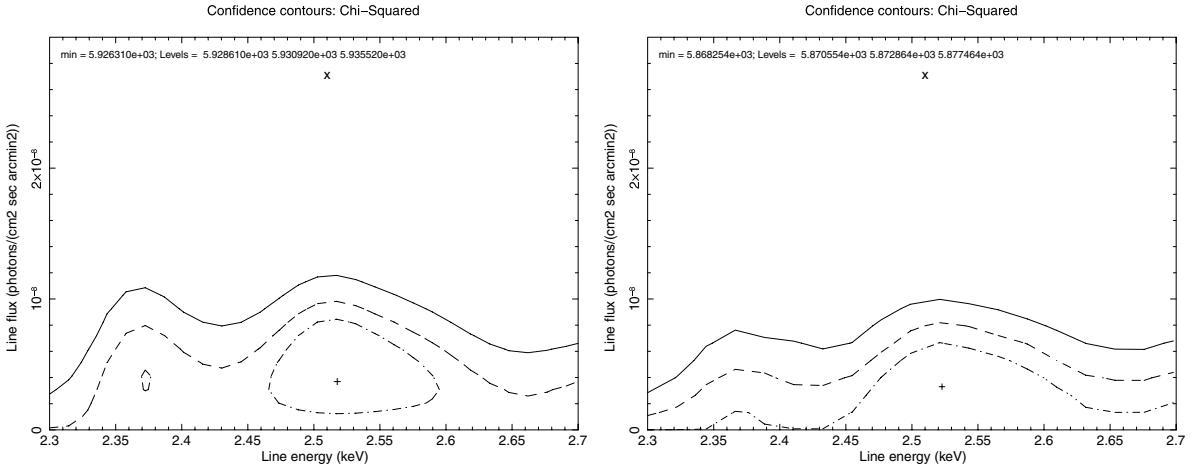

Figure 8. Left-hand panel: $\Delta\chi^2 = 2.3$ (dash–dotted), 4.61 (dashed) and 9.21 (solid) contours (corresponding to 68 per cent, 90 and 99 per cent confidence intervals) for a thin Gaussian line allowed by the joint fit of M31out spectra used in this work. The resulting line normalizations are shown for an averaged DM column density in the M31out region (about $170\,M_\odot\,pc^{-2}$, including the Milky Way contribution). The rescaled LK10 line is marked with a cross x; its normalization is therefore $4.50\times10^{-8}\times\frac{170}{208.5+73.9}=2.71\times10^{-8}$ photons cm^{-2} s arcmin^{-2}. It is clearly seen that the hypothesis of DM origin for a LK10 line-like feature is excluded at extremely high significance, corresponding to more than $\approx10\sigma$ (see text). Right-hand panel: The same as in the left figure but with an addition of a bknpow/b component to model the contribution of the remaining soft proton contamination (see text). The break energy is fixed as 3.2 keV so no degeneracy with the parameters of the Gaussian is expected. The bknpow/b power-law indices at low and high energies are fixed to be the same for different cameras observing the same spatial region. The line significance drops below 1σ in this case.

of fit. The significance contours of the resulting 'line' (for M31out region) are shown on the left-hand panel in Fig. 8. In deriving these limits we allowed both the parameters of the background, the position of the line and its total normalization to vary (the latter from negative values). Finally, we added an unfolded broken power-law component bknpow/b to model a contribution of remaining soft proton flares (see e.g. Kuntz & Snowden 2008). The break energy was fixed as 3.2 keV so no degeneracy with the parameters of the Gaussian is expected. The bknpow/b power-law indices at low and high energies were fixed to be the same for different cameras observing the same spatial region. further improved the quality of fit and made the line detection totally insignificant (see the right-hand panel of Fig. 8 for details). Our analysis clearly suggests the instrumental origin of the line-like features at the energy range of 2.1–2.8 keV.

As a final note, we should emphasize that the *Chandra* ACIS instrument used in LK10 has the Ir absorption edges near 2.11 and 2.55 keV (see Mirabal & Nieto 2010 for additional discussion). They also report negative result of searching for the LK10 feature, in agreement with our findings.

7 CONCLUSION

In this work, we demonstrated that the DM decay line can be unambiguously distinguished from spectral features of other origin (astrophysical or instrumental) by studying its spacial distribution. Many DM-containing objects would provide a comparable DM decay signal (Boyarsky et al. 2006b, 2009a; Bertone et al. 2007) which makes such a study possible (cf. Boyarsky, Ruchayskiy & Shaposhnikov 2009b; den Herder et al. 2009; Riemer-Sorensen & Hansen 2009). If an interesting candidate line is found in an object with an unusually high column density, the differences (always within an order of magnitude) in column densities with other objects can be compensated by longer exposure or bigger grasp of observing instruments.

To illustrate the power of this strategy, we have applied this approach to the recent result of LK10 who put forward a hypothesis about a decaying DM origin of an $\sim$2.51 keV spectral feature in *Chandra* observations of the Milky Way satellite known as Willman 1. Although the parameters of decaying DM, corresponding to such an interpretation, would lie in the region, already excluded at least 3σ level by several existing works (Watson et al. 2006; Abazajian et al. 2007; B08) we performed a new dedicated analysis of several archival observations of M31, Fornax and Sculptor dSphs.

The exclusions provided by M31 are extremely strong (at the level of 10σ–26σ, depending on the observed region). The 10σ bound is obtained using the off-centre (10–20 kpc) observations and a very conservative model of DM distribution with a heavy stellar disc and a very large ($\sim$28 kpc) DM core [the model of Corbelli et al. (2010), see Section 4.1]. Such a model leaves DM column density almost unchanged from about $\sim$30 kpc inwards. Combining all *XMM–Newton* observations of M31 at the distances 1–20 kpc off-centre provides more than 13σ bound assuming the model by Corbelli et al. (2010) and the 26σ bound with the model M31B of Widrow & Dubinski (2005) (with more physically motivated values of the mass of the stellar disc of M31).

Fornax dSph provides an exclusion between 3.3σ an 5σ (depending on how far from its nominal value 2.51 ± 0.07 keV the position of the line is allowed to shift) instead of $\sim4\sigma$ detection expected if the spectral feature of LK10 was of the DM origin. The bound of 3.3σ corresponds to the interval 2.3–2.72 keV and the 5σ exclusion corresponds to 2.44–2.58 keV interval.

To summarize, by comparing the strength and position of the feature found by Loewenstein & Kusenko with observations of several DM-dominated objects (M31, Fornax and Sculptor dSphs) we found that the hypothesis of DM origin of LK10 is excluded with the combined significance exceeding 14σ even under the most conservative assumptions. This is possible because of the large increase of the statistics in our observations as compared with the observation used in LK10.

To change this conclusion, a number of extreme (and not otherwise motivated) systematic errors would need to be present in determination of DM content of M31, Fornax and Sculptor dSph. The DM origin of the spectral feature of LK10 would remain consistent with existing archival data only if the DM amount in M31, Fornax and Sculptor are strongly overestimated and/or the mass of Willman 1 is grossly underestimated even compared to the best-fitting model of Strigari et al. (2008). It should be stressed that in our calculations of the expected signal in other objects, we have adopted for Willman 1 the DM column density that results from the mass modelling of Strigari et al. (2008). Our own modelling indicates that the mass of Willman 1 is highly uncertain. Even supposing that the measured velocity dispersion of Willman 1 provides a clean estimate of the mass, the general models of Walker et al. (2009a) allow the mass of Willman 1 to vary over several orders of magnitude within the region of interest. Furthermore, plausible scenarios such as tidal heating and/or contamination from unresolved binaries in the kinematic sample would cause the Willman 1 mass to be overestimated. We conclude that the column density derived from the modelling of Strigari et al. (2008) is approximately an upper limit. In contrast, the large kinematic samples of Fornax and Sculptor provide tighter mass constraints under the assumptions of our modelling, and given the larger inherent velocity dispersion, the modelling assumptions are more secure for Fornax and Sculptor than they are for Willman 1. As a result, we expect that significance of our exclusion of DM origin of LK10 feature to be very conservative.

Small line-like features (with the significance $\sim 2\sigma$) are present in the *XMM–Newton* spectrum at energies between 2 and 3 keV (see Fig. 8, left and Table 8 for details). Their most probable cause is the interaction of the satellite with soft protons (see discussion in Section 6) which can lead to an appearance of artificial spectral features due to the uncertainties in the effective area at these energies (cf. Kirsch et al. 2002, 2004). Indeed, the significance of the detection of these features drops below 1σ when the residual contamination with soft protons is modelled by an unfolded broken power law (see previous section for details).

The search for decaying DM is a well-motivated task, having crucial importance not only for cosmology and astrophysics, but also for particle physics. X-ray astronomy has a significant potential in this respect (Abazajian 2009; den Herder et al. 2009). Due to the small amount of baryons present in dwarf spheroidal galaxies, the uncertainties in DM determinations are smaller (as compared to e.g. spiral galaxies) and DM modelling provides tight bounds on the amount of DM. However, the above-mentioned uncertainties make Willman 1 (or other ultrafaint dwarfs) to be bad observational targets from the point of view of searching for decaying DM. On the contrary, the 'classical' dSphs provide excellent observational targets (Boyarsky et al. 2006b). A signal in Fornax, Sculptor (or other 'classical' dSphs such as Draco or Ursa Minor not considered here because of the absence of archival observations for them) would therefore have the potential to provide much more information about the nature of DM than would a signal from Willman 1. To improve significantly the best available bounds (see e.g. Boyarsky et al. 2009b) and to probe the most interesting region of parameter space,an extended (300–500 ks) observations of the well-studied dSphs are needed. However as we are searching for the weak diffuse signal, a special care should be taken in choosing the instruments and observational times in such a way that minimize possible flare contamination (see e.g. Boyarsky et al. 2007b). Drastic improvement in the decaying DM search is possible with a new generation of spectrometers, having large FOV and energy resolution close to several eV (Boyarsky et al. 2007a; Abazajian 2009; den Herder et al. 2009; Piro et al. 2009).

ACKNOWLEDGMENTS

We are grateful to L. Chemin, E. Corbelli, M. Markevitch, S. Molendi, J. Nevalainen, M. Shaposhnikov for many useful comments and discussions. DI is also grateful to Scientific and Educational Centre of the Bogolyubov Institute for Theoretical Physics in Kiev, Ukraine, and especially to V. Shadura, for creating wonderful atmosphere for young Ukrainian scientists. The work of AB and OR was supported in part by the Swiss National Science Foundation. The work of DI is supported in part from the SCOPES project no. IZ73Z0_128040 of Swiss National Science Foundation, the Cosmomicrophysics programme and the Program of Fundamental Research of the Physics and Astronomy Division of the National Academy of Sciences of Ukraine. The Dark Cosmology Centre is funded by the Danish National Research Foundation.

REFERENCES

Abazajian K., Fuller G. M., Tucker W. H., 2001, ApJ, 562, 593
Abazajian K. N., 2009, preprint (arXiv:0903.2040)
Abazajian K. N., Markevitch M., Koushiappas S. M., Hickox R. C., 2007, Phys. Rev. D, 75, 063511
Arnaud K., Dorman B., Gordon C., 2009, An X-Ray Spectral Fitting Package User's Guide for version 12.5.0, from http://heasarc.gsfc.nasa.gov/docs/xanadu/xspec/manual/manual.html
Asaka T., Blanchet S., Shaposhnikov M., 2005, Phys. Lett. B, 631, 151
Battaglia G. et al., 2005, MNRAS, 364, 433
Baudis L., 2007, preprint (arXiv:0711.3788)
Bell E. F., de Jong R. S., 2001, ApJ, 550, 212
Bell E. F., McIntosh D. H., Katz N., Weinberg M. D., 2003, ApJS, 149, 289
Bergstrom L., 2008, J. Phys. Conf. Ser., 120, 042005
Bertone G., Hooper D., Silk J., 2005, Phys. Rep., 405, 279
Bertone G., Buchmuller W., Covi L., Ibarra A., 2007, J, Cosmology Astropart. Phys., 0711, 003
Bezrukov F., Shaposhnikov M., 2007, Phys. Rev. D, 75, 053005
Boyarsky A., Ruchayskiy O., 2008, preprint (arXiv:0811.2385)
Boyarsky A., Neronov A., Ruchayskiy O., Shaposhnikov M., 2006a, Phys. Rev. D, 74, 103506
Boyarsky A., Neronov A., Ruchayskiy O., Shaposhnikov M., Tkachev I., 2006b, Phys. Rev. Lett., 97, 261302
Boyarsky A., den Herder J. W., Neronov A., Ruchayskiy O., 2007a, Astropart. Phys., 28, 303
Boyarsky A., Nevalainen J., Ruchayskiy O., 2007b, A&A, 471, 51
Boyarsky A., Iakubovskyi D., Ruchayskiy O., Savchenko V., 2008a, MNRAS, 387, 1361 (B08)
Boyarsky A., Malyshev D., Neronov A., Ruchayskiy O., 2008b, MNRAS, 387, 1345
Boyarsky A., Ruchayskiy O., Markevitch M., 2008c, ApJ, 673, 752
Boyarsky A., Ruchayskiy O., Iakubovskyi D., Maccio' A. V., Malyshev D., 2009a, preprint (arXiv:0911.1774)
Boyarsky A., Ruchayskiy O., Shaposhnikov M., 2009b, Annu. Rev. Nuclear Part. Sci., 59, 191
Buchmuller W., Covi L., Hamaguchi K., Ibarra A., Yanagida T., 2007, J. High Energy Phys., 03, 037
Bullock J. S., Johnston K. V., 2007, in de Jong R. S., ed., Island Universes, Dynamical Evolution of Accreted Dwarf Galaxies. Springer-Verlag, Berlin, p. 227
Burkert A., 1995, ApJ, 447, L25
Carr B. J., 2005, preprint (astro-ph/0511743
Carr J., Lamanna G., Lavalle J., 2006, Rep. Progress Phys., 69, 2475
Carter J. A., Read A. M., 2007, A&A, 464, 1155
Carter J. A., Sembay S., Read A. M., 2010, MNRAS, 402, 867

Chandra X-ray Centre 2009, CIAO 4.1 Science Threads, http://cxc.harvard.edu/ciao/threads/all.html
Chemin L., Carignan C., Foster T., 2009, ApJ, 705, 1395
Conlon J. P., Quevedo F., 2007, J. Cosmology Astropart. Phys., 0708, 019
Corbelli E., Lorenzoni S., Walterbos R. A. M., Braun R., Thilker D. A., 2010, A&A, 511, A89
De Luca A., Molendi S., 2004, A&A, 419, 837
den Herder J. W. et al., 2009, preprint (arXiv:0906.1788)
Diemand J., Kuhlen M., Madau P., 2007, ApJ, 667, 859
Dodelson S., Widrow L. M., 1994, Phys. Rev. Lett., 72, 17
Dolgov A. D., Hansen S. H., 2002, Astropart. Phys., 16, 339
Feng J. L., Rajaraman A., Takayama F., 2003, Phys. Rev. Lett., 91, 011302
Feng J. L., Su S.-f., Takayama F., 2004, Phys. Rev. D, 70, 063514
Fruscione A. et al., 2006, in Silva D. R., Doxsey R. E., eds, Proc. SPIE Conf. Ser. Vol. 6270, Observatory Operations: Strategies, Processes, and Systems. SPIE, Bellingham, p. 62701
Geehan J. J., Fardal M. A., Babul A., Guhathakurta P., 2006, MNRAS, 366, 996
Hargreaves J. C., Gilmore G., Annan J. D., 1996, MNRAS, 279, 108
Hickox R. C., Markevitch M., 2006, ApJ, 645, 95
Hooper D., 2009, preprint (arXiv:0901.4090)
Hooper D., Baltz E. A., 2008, Annu. Rev. Nuclear Part. Sci., 58, 293
Irby B., 2008, The ftools webpage, HeaSoft, http://heasarc.gsfc.nasa.gov/docs/software/ftools/ftools_menu.html
Jeltema T. E., Profumo S., 2008, ApJ, 686, 1045
Kerins E., 2004, MNRAS, 347, 1033
Kerins E. et al., 2001, MNRAS, 323, 13
Kirsch M. G. F. et al., 2002, EPIC Status of Calibration and Data Analysis (XMM-SOC-CAL-TN-0018), http://xmm.vilspa.esa.es/docs/documents/CAL-TN-0018-2-0.pdf
Kirsch M. G. F. et al., 2004, in Hasinger G., Turner M. J. L., eds, Proc. SPIE Conf. Ser. Vol. 5488, XMM-Newton (Cross)-Calibration. SPIE, Bellingham, p. 103
Klypin A., Zhao H., Somerville R. S., 2002, ApJ, 573, 597
Kuntz K. D., Snowden S. L., 2008, A&A, 478, 575
Kusenko A., Loewenstein M., 2010, preprint (arXiv:1001.4055)
Lattanzi M., Valle J. W. F., 2007, Phys. Rev. Lett., 99, 121301
Leccardi A., Molendi S., 2008, A&A, 486, 359
Lee B. W., Weinberg S., 1977, Phys. Rev. Lett., 39, 165
Loewenstein M., Kusenko A., 2010, ApJ, 714, 652 (LK10)
Loewenstein M., Kusenko A., Biermann P. L., 2009, ApJ, 700, 426
Lumb D. H., Warwick R. S., Page M., De Luca A., 2002, A&A, 389, 93
Markevitch M., 2009, http://cxc.harvard.edu/ciao/contrib/bg
Markevitch M., Bautz M. W., Biller B. et al., 2003, ApJ, 583, 70
Martin N. F., Ibata R. A., Chapman S. C., Irwin M., Lewis G. F., 2007, MNRAS, 380, 281
Martin N. F., de Jong J. T. A., Rix H.-W., 2008, ApJ, 684, 1075
Mateo M. L., 1998, ARA&A, 36, 435
Mateos S., Saxton R. D., Read A. M., Sembay S., 2009, A&A, 496, 879
Mirabal N., Nieto D., 2010, preprint (arXiv:1003.3745)
Moretti A., Pagani C., Cusumano G. et al., 2009, A&A, 493, 501
Navarro J. F., Frenk C. S., White S. D. M., 1997, ApJ, 490, 493
Nevalainen J., Markevitch M., Lumb D., 2005, ApJ, 629, 172
Olszewski E. W., Aaronson M., Hill J. M., 1995, AJ, 110, 2120
Peñarrubia J., McConnachie A., Navarro J. F., 2008, ApJ, 672, 904
Peñarrubia J., Navarro J. F., McConnachie A. W., Martin N. F., 2009, ApJ, 698, 222
Piro L., den Herder J. W., Ohashi T. et al., 2009, Exp. Astron., 23, 67
Pradas J., Kerp J., 2005, A&A, 443, 721
Read A. M., Ponman T. J., 2003, A&A, 409, 395
Riemer-Sørensen S., Hansen S. H., 2009, A&A, 500, L37
Seigar M. S., Barth A. J., Bullock J. S., 2008, MNRAS, 389, 1911
Siegel M. H., Shetrone M. D., Irwin M., 2008, AJ, 135, 2084
Stanek K. Z., Garnavich P. M., 1998, ApJ, 503, L131
Strigari L. E. et al., 2006, ApJ, 652, 306
Strigari L. E., Koushiappas S. M., Bullock J. S., Kaplinghat M., Simon J. D., Geha M., Willman B., 2008, ApJ, 678, 614
Takayama F., Yamaguchi M., 2000, Phys. Lett. B, 485, 388
Tempel E., Tamm A., Tenjes P., 2007, preprint (arXiv:0707.4374)
Walker M. G., Mateo M., Olszewski E. W., Peñarrubia J., Wyn Evans N., Gilmore G., 2009a, ApJ, 704, 1274
Walker M. G., Mateo M., Olszewski E. W., 2009b, AJ, 137, 3100
Walterbos R. A. M., Kennicutt R. C. Jr, 1987, A&AS, 69, 311
Walterbos R. A. M., Kennicutt R. C. Jr, 1988, A&A, 198, 61
Watson C. R., Beacom J. F., Yuksel H., Walker T. P., 2006, Phys. Rev. D, 74, 033009
Widrow L. M., Dubinski J., 2005, ApJ, 631, 838
Willman B. et al., 2005, ApJ, 626, L85

This paper has been typeset from a TEX/LATEX file prepared by the author.